APPLICATION OF A MULTI-PARAMETER TRANSFORMATION FOR DEFORMATION MONITORING OF A LARGE STRUCTURE

Bill Teskey and Bijoy Paul
Department of Geomatics Engineering, University of Calgary, Alberta, CANADA
Email: wteskey@ucalgary.ca, bpaul@ucalgary.ca

Bill. Lovse
Terramatic Technologies Inc., Calgary, Alberta, CANADA
Email: b.lovse@terramatic.com

Abstract: A new methodology for deformation monitoring is applied to a large structure. The mathematical model for the new methodology utilizes a multi-parameter transformation relating original and repeated observations between an instrument station and any number of target points. The mathematical model is applied to original and repeated reflectorless total station observations made to target points in the roof of the Olympic Speedskating Oval in Calgary. (The Olympic Oval roof structure, with an unsupported roof span of approximately 80m by 200m, is one of the largest of its type in the world.) Results from this application indicate that the new methodology is very effective for deformation monitoring. Future work will include application of the new methodology to original and repeated three-dimensional laser scanner observations. The challenge with laser scanner observations (point clouds) is to match identical features in original and repeated point clouds. Recent research work in least squares orthogonal distance fitting of curves and surfaces in space may offer a solution to this problem.

1. Introduction

A new methodology for deformation monitoring is investigated by applying it to a large structure. The mathematical model for the new methodology is described in Section 2. Application of the new methodology, through an analysis of original and repeated reflectorless total station observations to target points on a large roof structure, is described in Section 3. A strategy for applying the new methodology to original and repeated three-dimensional laser scanner observations, is outlined in Section 4.

2. Mathematical Model

The mathematical model for the new methodology utilizes an multi-parameter transformation relating original and repeated observations between an instrument station (e.g. total station or three-dimensional laser scanner) and any number of target points. The transformation consists of a 6-parameter similarity transformation at the instrument station (translations in the X-, Y- and Z-directions at the instrument station, and rotations about the X-, Y- and Z-axes at the instrument station), plus a scale factor relating original and repeated instrument-target slope distance observations (or derived slope distance observations), plus a refraction correction between original and repeated zenith angle observations (or derived zenith angle observations).

This mathematical model can be expressed as follows:

$$X_O = \lambda(X_R + \kappa Y_R - \varphi Z_R) + T_x \quad (1)$$

$$Y_O = \lambda(-\kappa X_R + Y_R + \omega Z_R) + T_y \quad (2)$$

$$Z_O = \lambda(\varphi X_R - \omega Y_R + Z_R) + T_z \quad (3)$$

with $X_R = S_R \sin H_R \sin(V_R + (\Delta R) S_R)$ (4)

$$Y_R = S_R \cos H_R \sin(V_R + (\Delta R) S_R) \quad (5)$$

$$Z_R = S_R \cos(V_R + (\Delta R) S_R) \quad (6)$$

$$X_O = S_O \sin H_O \sin V_O \quad (7)$$

$$Y_O = S_O \cos H_O \sin V_O \quad (8)$$

$$Z_O = S_O \cos V_O \quad (9)$$

in which H_O, V_O and S_O are original horizontal circle, vertical circle (zenith angle) and slope distance observations (or derived observations) respectively;

H_R, V_R and S_R are repeated horizontal circle, vertical circle (zenith angle) and slope distance observations (or derived observations) respectively;

X_O, Y_O and Z_O are X-, Y- and Z-coordinates computed from the original observations;

X_R, Y_R and Z_R are X-, Y- and Z-coordinates computed from the repeated observations;

T_x, T_y and T_z are X-, Y- and Z-translations respectively at the instrument station;

ω, φ and κ are rotations about the X-, Y- and Z-axes respectively at the instrument station;

λ is the scale factor relating original and repeated slope distance observations; and ,

ΔR is the refraction correction (in arc seconds per metre of slope distance; see reference [6]) relating original and repeated zenith angle observations (or derived observations).

The set of equations (1) through (9) inclusive can be solved as an implicit nonlinear least squares adjustment to obtain the transformation parameters ω, φ, κ, T_x, T_y, T_z, λ and ΔR; corrected observations H_O, V_O, S_O, H_R, V_R and S_R to each target point; and movements (X_T - X_O), (Y_T -Y_O) and (Z_T - Z_O) of each target point.(X_T, Y_T and Z_T are transformed X-, Y- and Z-coordinates as given by the right-hand-sides of Equations (1), (2) and (3) respectively.)

3. Application of the Multi-Parameter Transformation: Olympic Oval Roof

3.1 Background

The Olympic Speedskating Oval in Calgary is a very large, uniquely designed structure. It was built for the 1988 Winter Olympics. The Olympic Oval roof structure, with an

unsupported span of approximately 80m by 200m, is one of the largest of its type in the world.

The roof structure of the Olympic Oval consists of 84 interconnected hollow-core beam columns. The external cross section of the beam columns is approximately 1m wide by 2m deep. The roof structure is hinged at the tops of buttressed columns, with both the columns and buttresses founded on concrete piles. The columns are approximately 1.5m in diameter and the buttresses are approximately 1.5m wide by 2m deep. Fig. 1(a) shows a cross section through the Olympic Oval and Fig. 1(b) shows the west elevation.

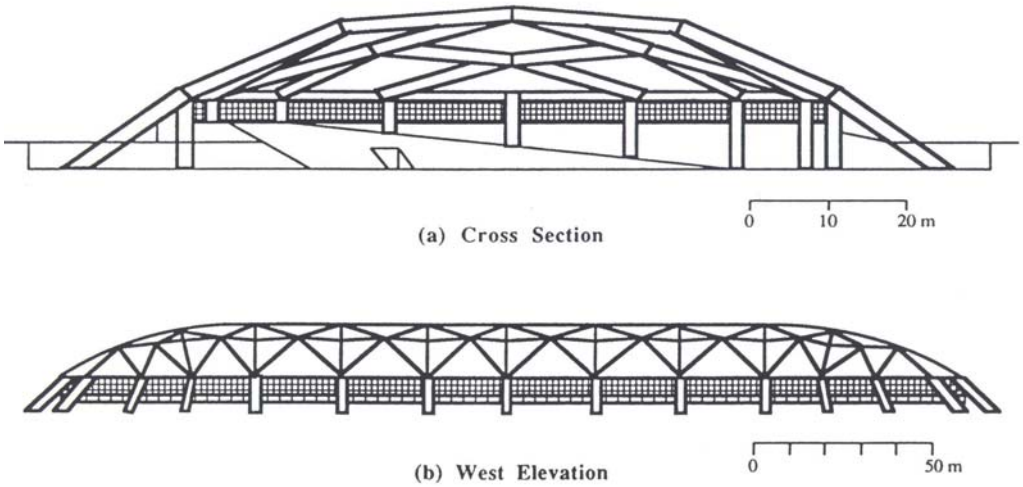

Figure 1 – Olympic Oval, Calgary

The Olympic Oval has experienced both short-term and long-term deformations. The short-term deformations (deformations occurring as soon as the load is applied) are due to:

1. Dead weight load of the structure itself.
2. Snow load on the structure.
3. Wind load on the structure.
4. Temperature changes in the structure.

The long-term deformations are due to:

1. Shrinkage of the concrete.
2. Creep of the concrete and soil (progressively smaller deformations occurring over a period of time under constant loading conditions).
3. Changes in soil stiffness because of variations in moisture content of the soil.

The first deformations of interest (those due to the dead weight load of the roof structure) occurred when the roof structure was lowered onto the buttressed column substructure in June 1986. An analysis of these deformations is summarized in [7]. Deformations of interest which occurred after the June 1986 dead weight load deformations were those due to creep and shrinkage of the concrete in the roof beam columns. An analysis of these deformations is also summarized in [7].

3.2 Deformation Monitoring

In recent years, the only significant deformations in the Olympic Oval are vertical movements of the roof structure caused by seasonal temperature variations. A detailed analysis of these deformations is given in [7].

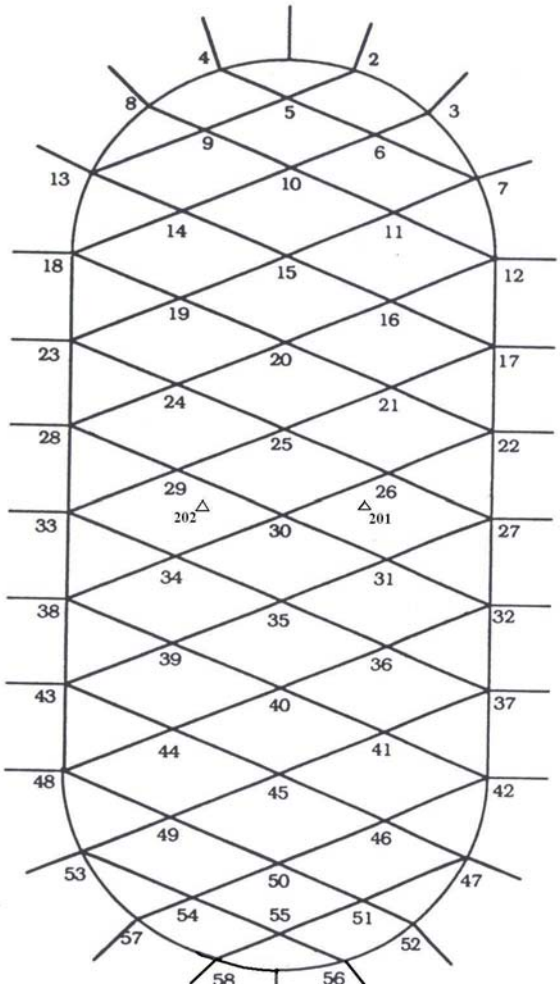

Figure 2 – Plan View of Olympic Oval Roof

Based on the known seasonal movement of the Olympic Oval roof structure, it was planned to apply the multi-parameter transformation to an epoch of original observations made in July 2005 (outside temperature about +30 degrees Celcius) and an epoch of repeated observations made in January 2006 (outside temperature about -30 degrees Celcius). Unfortunately, January 2006 and the first two weeks of February 2006 were unseasonably warm. It was therefore decided to apply the multi-parameter transformation to two other epochs of observations (original and repeated), one made on July 4, 2005 and the other made on July 6, 2005.

A small subset of original and repeated reflectorless total station observations are shown in Table 1, with horizontal circle observations denoted as H, vertical circle observations denoted

as V, and slope distance observations denoted as S. These observations were made from the floor of the Olympic Oval at point 201 to roof points 5, 10, 15, 20, 25 and 30; see Figure 2. The measurements were made with a Leica TCR 803 reflectorless total station. Estimated standard deviations of the total station observations are +/- 2 arc seconds for horizontal and vertical circle observations, and +/- 2mm for slope distance observations.

Roof Point	H(dms)	V(dms)	S(m)
5/Original	351-28-49	80-48-41	87.301
5/Repeated	351-28-58	80-47-19	87.306
10/Original	348-59-35	75-20-55	74.825
10/Repeated	348-59-47	75-19-24	74.834
15/Original	344-45-39	68-19-00	56.956
15/Repeated	344-45-48	68-17-01	56.969
20/Original	337-09-55	60-41-26	42.816
20/Repeated	337-10-07	60-39-04	42.833
25/Original	314-51-44	46-47-26	30.629
25/Repeated	314-51-50	46-44-31	30.653
30/Original	260-28-12	38-41-27	26.858
30/Repeated	260-28-16	38-38-44	26.885

Table 1 – Reflectorless Total Station Observations to Olympic Oval Roof Points

3.3 Analysis and Results

The mathematical model described in Section 2 was used to recover the deformations. In this application, rotations ω and φ were set to zero because the total station has dual axis compensation. Translations T_x and T_y were also set to zero because the total station was centered over the same point for original and repeated observations. Scale factor λ and refraction correction ΔR were dealt with as free parameters since one could reasonably expect different atmospheric conditions on July 4 and July 6. Rotation κ was dealt with as a free parameter to allow rotation in the horizontal plane.

The results from the application of the mathematical model to recover movements are shown in Tables 2a, 2b and 2c. These results show that the movement of the roof points (zero movement) was recovered by the mathematical model described in Section 2.

Location	Movement(mm)	Stn Dev(mm)	Significant ?
Roof Point 5	**$(Z_T - Z_O) = + 0.2$**	**+/- 0.3**	**No**
Roof Point 10	**$(Z_T - Z_O) = - 0.3$**	**+/- 0.3**	**No**
Roof Point 15	**$(Z_T - Z_O) = + 0.4$**	**+/- 0.3**	**No**
Roof Point 20	**$(Z_T - Z_O) = - 0.3$**	**+/- 0.2**	**No**
Roof Point 25	**$(Z_T - Z_O) = + 0.3$**	**+/- 0.3**	**No**
Roof Point 30	**$(Z_T - Z_O) = - 0.3$**	**+/- 0.3**	**No**

Table 2a – Recovered Z-Movements, Olympic Oval

Location	Movement(mm)	Stn Dev(mm)	Significant ?
Roof Point 5	**$(X_T - X_O) = + 0.1$**	**+/- 0.2**	**No**
Roof Point 10	**$(X_T - X_O) = + 0.1$**	**+/- 0.2**	**No**
Roof Point 15	**$(X_T - X_O) = - 0.4$**	**+/- 0.2**	**No**
Roof Point 20	**$(X_T - X_O) = + 0.1$**	**+/- 0.2**	**No**
Roof Point 25	**$(X_T - X_O) = + 0.1$**	**+/- 0.2**	**No**
Roof Point 30	**$(X_T - X_O) = + 0.1$**	**+/- 0.2**	**No**

Table 2b – Recovered X-Movements, Olympic Oval

Location	Movement(mm)	Stn Dev(mm)	Significant ?
Roof Point 5	**$(Y_T - Y_O) = + 0.2$**	**+/- 0.4**	**No**
Roof Point 10	**$(Y_T - Y_O) = - 0.3$**	**+/- 0.4**	**No**
Roof Point 15	**$(Y_T - Y_O) = + 0.4$**	**+/- 0.4**	**No**
Roof Point 20	**$(Y_T - Y_O) = - 0.3$**	**+/- 0.3**	**No**
Roof Point 25	**$(Y_T - Y_O) = + 0.3$**	**+/- 0.3**	**No**
Roof Point 30	**$(Y_T - Y_O) = - 0.3$**	**+/- 0.3**	**No**

Table 2c – Recovered Y-Movements, Olympic Oval

4. Strategy for Applying Multi-Parameter Transformation to Laser Scanner Observations

4.1 Work to Date

Results from the application of the multi-parameter transformation to *planned* three-dimensional laser scanner observations in a typical industrial survey application (see Figure 3) are shown in Table 3 and reported in [8]. Estimated standard deviations of laser scanner observations (+/- 5 arc seconds and +/- 1 mm) are given in [4] and [5].

The problem with this analysis is that points R1 to R18 inclusive in Figure 3 must be circular or spherical target points. In an actual application it would be far too time-consuming to set these points each time observations were made.

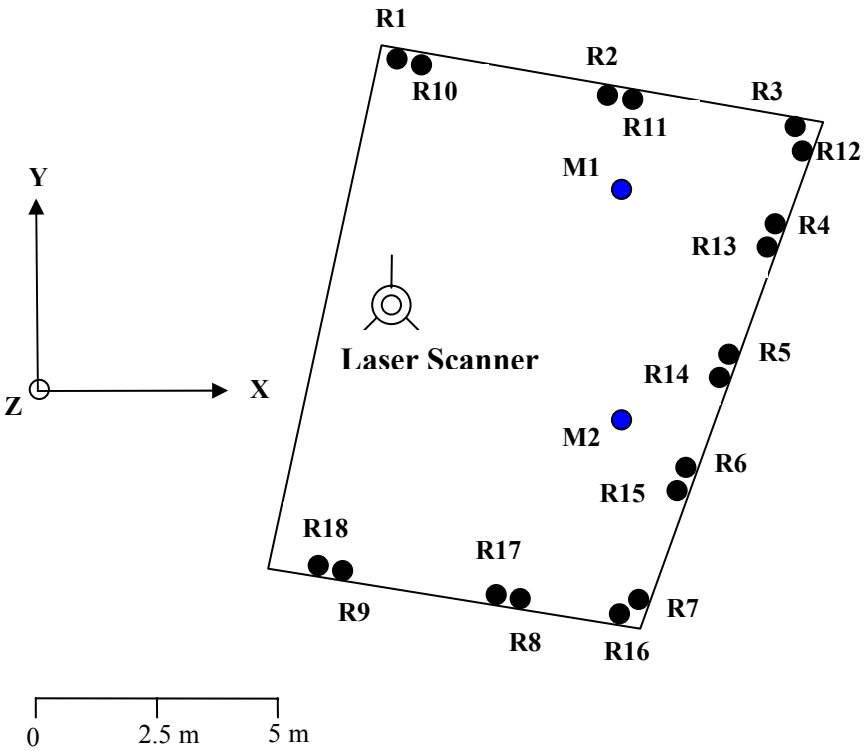

Figure 3 – Plan View of Location of Target Points at Indoor Industrial Site

Location	Standard Deviation of Movement(mm or arcsecs)	Standard Deviation of Mean Position(mm)
Machine Point M1	**$(X_T - X_O)$: +/- 0.14**	**$(X_T + X_O)/2$: +/- 0.07**
Machine Point M1	**$(Y_T - Y_O)$: +/- 0.24**	**$(Y_T + Y_O)/2$: +/- 0.12**
Machine Point M1	**$(Z_T - Z_O)$: +/- 0.36**	**$(Z_T + Z_O)/2$: +/- 0.18**
Machine Point M2	**$(X_T - X_O)$: +/- 0.14**	**$(X_T + X_O)/2$: +/- 0.07**
Machine Point M2	**$(Y_T - Y_O)$: +/- 0.24**	**$(Y_T + Y_O)/2$: +/- 0.12**
Machine Point M2	**$(Z_T - Z_O)$: +/- 0.36**	**$(Z_T + Z_O)/2$: +/- 0.18**
Laser Scanner	**ω: +/- 2.6**	**---**
Laser Scanner	**φ: +/- 5.3**	**---**
Laser Scanner	**κ: +/- 2.7**	**---**
Laser Scanner	**T_x: +/- 0.07**	**---**
Laser Scanner	**T_y: +/- 0.12**	**---**
Laser Scanner	**T_z: +/- 0.18**	**---**

Table 3 – Standard Deviations of Movements and Mean Positions, Indoor Industrial Site

4.2 Strategy

The strategy to overcome the problem described in Section 4.1 is to match identical features in original and repeated laser scanner observations (point clouds). For man-made structures, the intersection of three or more angular surfaces might work well [3]. For natural structures, generation of virtual points of maximum curvature may be the only alternative. Recent research work in least squares orthogonal distance fitting of surfaces in space [1] [2] provides information on how virtual points of identical natural features might be generated.

5. Conclusion

The results indicate that the new methodology is very effective for deformation monitoring utilizing reflectorless total station observations. The new methodology for deformation monitoring should also be very effective utilizing three-dimensional laser scanner observations, once some interesting technical challenges are overcome.

Acknowledgements

The authors would like to thank Kameron Kiland for arranging access to the Olympic Oval facility. The authors also wish to acknowledge Dr. Robert Radovanovic who works closely with us in our high-precision industrial surveys research.

References

[1] Ahn, S. J. (2004). "Least Squares orthogonal Distance Fitting of Curves and Surfaces in Space", Lecture Notes in Computer Science, Springer, Berlin, 128pp.

[2] Akca, D. and Gruen, A. (2005). "Recent Advances in Least Squares Surface Matching", Proceedings of Optical 3D Measurement Techniques VII, Vienna, October 3-5, Vol. II, pp. 197-206.

[3] Lindenbergh, R. and Pfeifer, N. (2005)."A Statistical Deformation Analysis of Two Epochs of Terrestrial Laser Scanner Data of a Lock", Proceedings of Optical 3D Measurement Techniques VII, Vienna, October 3-5, Vol. II, pp. 61-70.

[4] Mensi (2004). "GS200 Declaration of Conformity", Mensi 3D Surveying Products, Fontenay-Sous-Bois, France, 3 pp.

[5] Rueger, J. M. (2003). "Electronic Surveying Instruments", Monograph 18, School of Surveying and Spatial Information Systems, The University of New South Wales, Sydney, 155 pp.

[6] Rueger, J. M. (1993). "Monitoring of Slope Movements Using Electronic Distance Measurements and Precision Theodolites", Proceedings of the 35th Australian Surveyors' Congress, pp. 19-38.

[7] Teskey, W. F., Radovanovic, R. S., Paul, B. and Brazeal, R. G. (2004). "Measurement of Temperature-Induced Deformations in a Large Roof Structure", Proceedings of the 1st International FIG Symposium on Engineering Surveys for Construction Works and Structural Engineering, Nottingham, United Kingdom, June 28 – July 1, 15 pp.

[8] Teskey, W.F., Paul B. and Lovse, J.W. (2005). "New Instrumentation and Methodology for Deformation Monitoring", Proceedings of the 7th Conference on Optical 3-D Measurement Techniques", Vienna, October 3-5, 9 pp.